The effect of Nb, Ti introduction sequence on the adsorption of Nb on TiB₂ surface and grain refinement performance of Al-4Ti-1Nb-1B

Hao Yia,b, Ying Chenga,b,*, Huarui Zhanga,b,*, Hu Zhanga,b

a. School of Materials Science and Engineering, Beihang University, Beijing 100191, China
 B. Ningbo Institute of Technology (NIT), Beihang University, Ningbo 315000, China
 * Corresponding author.

E-mail address: huarui@buaa.edu.cn (H. Zhang), 11018@buaa.edu.cn (Y. Cheng).

Abstract: In recent years, Al-Ti-Nb-B grain refiners have attracted increasing attention due to their grain refinement performance and anti Si-poisoning ability. This study investigates the influence of the introduction sequence of Ti and Nb during the synthesis of Al-4Ti-1Nb-1B refiners on their refinement performance and Si poisoning resistance. It is found that Al-4Ti-1Nb-1B prepared by introducing Ti prior to Nb exhibits the best grain refinement and anti-Si poisoning properties, refining Al-7Si to $150.12 \pm 27.5 \, \mu m$. This superior performance is attributed to the fact that the variation in ground-state energy ΔE for the Ti prior to Nb sequence is lower than that of other sequences, thereby facilitating Nb adsorption on the TiB₂ surface. TEM observations corroborate these findings, showing that TiB₂ prepared by this sequence has the highest average Nb content of 3.80 at.%. First-principles calculations reveal that this unique Nb adsorption enhances the TiB₂/Al interfacial adhesion energy W_{ad} and suppresses the segregation tendency of Si atoms at the interface, $\kappa_{Si}(c_{Si})$. The higher the Nb adsorption at the TiB₂/Al interface, the stronger the resistance to Si poisoning. These findings underscore the pivotal role of Nb-modified TiB₂ in improving grain refinement and offer a novel strategy for advancing grain refiner technologies in Al-Si alloys.

Keywords: Introduction sequence, grain refinement, Nb adsorption, nucleation mechanism.

1 Introduction

Cast Al-Si alloys are widely used in modern industries, aerospace, aviation, construction, transportation, due to their excellent castability, lightweight nature, and corrosion resistance [1-4]. During the casting of Al-Si alloys, grain refinement is a critical process, as it effectively refines primary α-Al grains, thereby improving both the castability and mechanical properties of the alloys [5, 6]. Currently, the most common grain refinement strategy involves the addition of grain refiners into the Al-Si melt [7, 8], Among which the Al-5Ti-1B grain refiner is the most extensively used. However, during practical applications, the presence of Si in the Al-Si melt can lead to the formation of silicides, such as TiSi2 and Ti5Si3 on the surface of TiB2 particles in Al-5Ti-1B [9, 10]. These silicides inhibit the heterogeneous nucleation of α-Al, resulting in a significant deterioration of grain refinement performance in Al-Si alloys [11, 12], especially Al-Si alloys with Si content exceeding 5 wt.%, which is commonly known as the Si-poisoning effect.

In recent years, novel grain refiners have been developed to overcome the issue of Si-poisoning in Al-Si

alloys. Nb has attracted attention due to its ability to form NbAl₃ and NbB₂ phases, which are analogous to TiAl₃ and TiB2 in Al-5Ti-1B. Consequently, Al-Nb-B grain refiners were developed and have demonstrated better grain refinement performance in Al-Si alloys compared to conventional Al-5Ti-1B refiners [13-15]. improvement is primarily attributed to the higher thermodynamic stability of NbAl₃ compared to TiAl₃, which makes it less reactive with Si to form Nb-based silicides such as NbSi₂, Nb₃Si, and Nb₅Si₃ [16-18]. However, the limited anti-fading performance of Al-Nb-B restricts its widespread industrial application [19, 20]. To address this limitation, researchers have attempted to integrate the advantages of both Ti and Nb, leading to the development of Al-Ti-Nb-B grain refiners. Xu et al. [21] developed an Al-1.67Ti-3.33Nb-0.5B refiner and reported that (Nb, Ti)B₂ particles acted as highly effective heterogeneous nucleation sites for α-Al in Al-Si alloys. Li et al. [22, 23] introduced Ti into the Al-Nb-B melt, forming (Nb, Ti)B2 core-shell structure with TiB2 as the core and NbB2 as the shell, which also exhibited excellent resistance to Si poisoning. Wu et al. [24]

synthesized an Al-3.5Nb-1Ti-1B refiner containing (Ti, Nb)B₂ particles with a distinctive sandwich-like Nb-Ti-Nb structure, achieving notable refinement performance in Al-Si alloys. Additionally, Li et al. ^[25-27] developed the TCB refiner based on the Al-Ti-B-C system, and Xue et al. ^[28] proposed an Al-4.2V-1.8B refiner. Both refiners also demonstrated excellent refinement efficiency in Al-Si alloys and provide valuable insights into overcoming Si poisoning.

Among these recently developed grain refiners, Al-Ti-Nb-B has emerged as a promising and significant candidate. Our previous study [29] observed a nanoscale Nb adsorption layer on the (0110) plane of TiB₂, which can activate TiB₂ as an effective heterogeneous nucleus for α-Al. The composition design and processing parameters significantly influence the morphology and structure of the resulting borides. Ti and Nb are the two most critical refining elements in the Al-Ti-Nb-B system, and the sequence in which they are introduced plays a crucial role in achieving Nb adsorption on the TiB₂ surface, thereby affecting both the grain refinement efficiency and Si-poisoning resistance.

In this study, Al-4Ti-1Nb-1B grain refiners were prepared via different sequences for introducing Ti and Nb to investigate their influence on Nb adsorption at the TiB₂ surface and refinement performance. The grain refinement performance of the prepared refiners were evaluated on CP-Al, Al-3.5Si, Al-7Si, and Al-10.5Si alloys. The Nb adsorption behavior on the TiB₂ surface was quantitatively characterized and compared via TEM

and EDS line-scanning techniques. First-principles calculations were further applied to elucidate the mechanisms underlying Nb atom adsorption and its impact on grain refinement performance and Si-poisoning resistance. These findings provide valuable guidance for the innovative design of Al-Ti-Nb-B grain refiners and contribute to the development of more efficient grain refinement strategies for Al-Si alloys.

2 Experiment method

2.1 Preparation process of Al-4Ti-1Nb-1B master alloys

A series of Al-Ti-Nb-B alloys were synthesized via different Nb and Ti introduction sequences. Al-10Ti and Al-8B master alloys were first put into a SiC crucible at a stoichiometric Ti/B ratio of 2.2 and melted at 800 °C. The melt was stirred and held for 30 min to ensure the complete formation of TiB₂. Subsequently, as illustrated in Fig. 1, Al-10Nb and Al-10Ti were introduced into the melt in three different sequences, followed by an increase in temperature to 900 °C. Fig. 1(a) shows the process in which Nb was added prior to Ti; the resulting refiner is labeled as A-Al-4Ti-1Nb-1B (hereafter referred to as Sample A). In contrast, Fig. 1(b) depicts the process where Ti was added before Nb, producing a refiner designated as B-Al-4Ti-1Nb-1B (Sample B). Fig. 1(c) illustrates the simultaneous addition of Ti and Nb, resulting in C-Al-4Ti-1Nb-1B (Sample C). During the holding time, all melts were stirred using a graphite rod at a constant rotation speed. Finally, the melt was poured into a plate-shaped mold preheated to 200 °C.

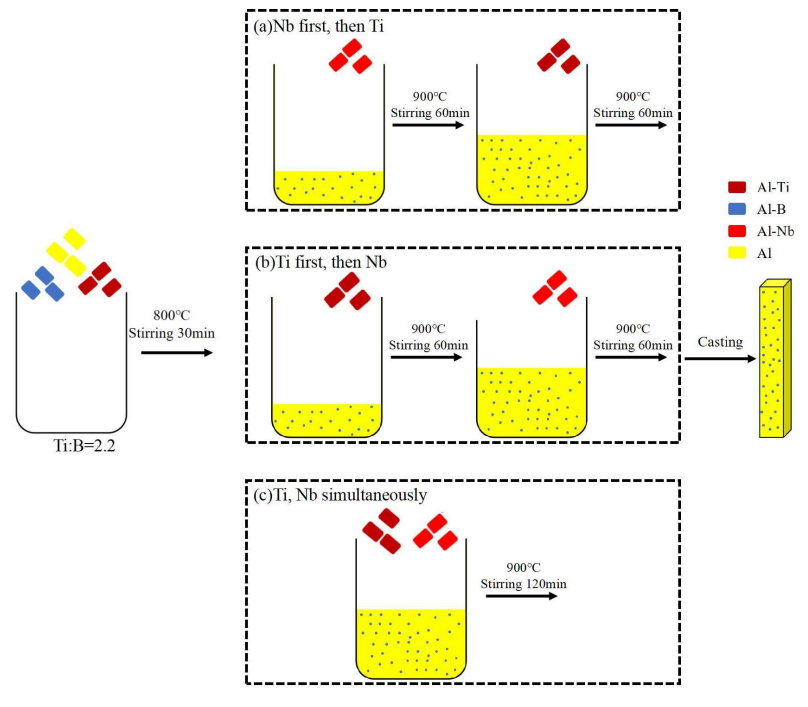


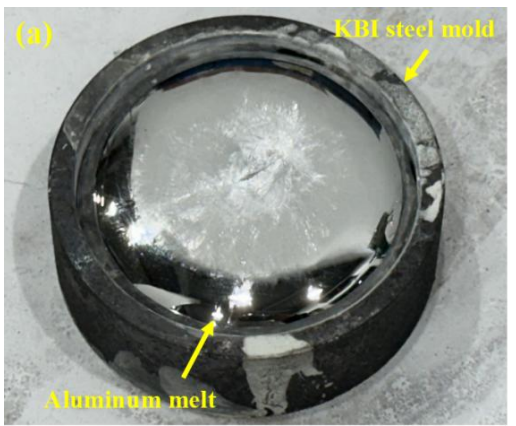
Fig. 1 Schematic diagram of the processing route for introducing Nb and Ti

2.2 Grain refinement experiments of Al-4Ti-1Nb-1B master alloys

To comprehensively evaluate the grain refinement performance of Al-4Ti-1Nb-1B prepared with different Nb and Ti introduction sequences, a series of Al-Si alloys (CP-Al, Al-3.5Si, Al-7Si, and Al-10.5Si) were fabricated by melting CP-Al (≥99.9%) with Al-20Si alloys. To modify the eutectic Si phase, 0.2 wt.% Al-10Sr was added, followed by the addition of 0.5 wt.% Al-4Ti-1Nb-1B grain refiners at 720 °C. The melt was immediately stirred with a graphite rod for 1 min to promote complete melting and uniform dispersion of the grain refiness, and held for 2 min. Then the melt was cast into a KBI cylindrical steel mold (Φ 75 mm × 25 mm) [30], which was placed on a refractory brick preheated to 200 °C, as illustrated in Fig. 2. The cooling rate under

this solidification condition was approximately 0.4 °C/s. For comparison, a commercial Al-5Ti-1B refiner (provided by AMG) was also conducted under same casting conditions to refine the Al-Si alloys. The detailed parameters for the grain refinement experiments are summarized in Table 1.

To accurately determine the grain size of the refined α -Al phase, the surfaces of the aluminum ingots in contact with the refractory brick were ground and polished. An electrolytic corrosion test was conducted using a WY-06 model apparatus, applying an anode coating with a 1 wt.% fluoboric acid solution. The α -Al grain size was observed using a polarized optical metallographic microscope (SG-51) and measured by the mean linear intercept method in accordance with ASTM E112-10.



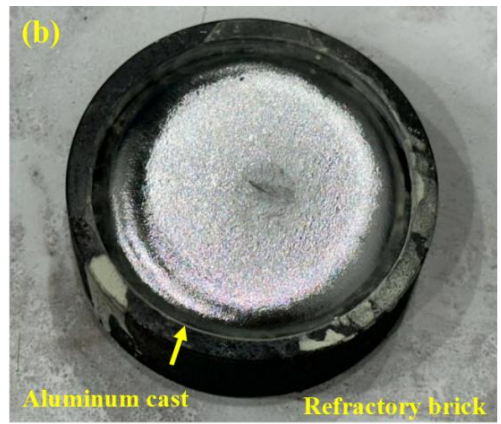


Fig 2 KBI standard solidification experiment: (a) Aluminum melt poured into KBI ring mold; (b) Solidified aluminum casting.

Table 1 Experimental parameters of grain refinement.

Grain refiner	Addition level/wt.%	Aluminum
		CP-Al
C1- A	0.5	Al-3.5Si
Sample A		Al-7Si
		Al-10.5Si
		CP-Al
Sample B	0.5	Al-3.5Si
		Al-7Si
		Al-10.5Si
	0.5	CP-Al
Sample C		Al-3.5Si
		Al-7Si
		Al-10.5Si
	0.5	CP-Al
Al-5Ti-1B		Al-3.5Si
		Al-7Si
		Al-10.5Si

2.3 Characterization of Al-4Ti-1Nb-1B master alloys

Samples were sectioned from Al-4Ti-1Nb-1B. After ground and polished, the microstructure of the Al-4Ti-1Nb-1B was observed using a field emission scanning electron microscope (Phenom-XL G2), and elemental distribution was analyzed via the integrated energy-dispersive X-ray spectroscopy (EDS). To precisely investigate Nb adsorption on the surface of particles, site-specific slices TiB_2 containing representative TiB₂ particles were prepared by focused ion beam (FIB) milling using a Helios G4 CX system. The particle structure and elemental adsorption at nucleation sites were further examined by transmission electron microscopy (Talos F200X).

2.4 First-principle calculations

First-principles calculations based on the density functional theory (DFT) were performed using the Vienna Ab-initio Simulation Package (VASP) in this study [31-35]. Perdew-Burke-Ernzerhof (GGA-PBE) exchange correlation functional was used to calculate the electronic correlation function, and conjugate gradient algorithm was applied to optimize the geometry. The plane-wave cutoff energy of diboride/Al interface system was set to be 450 eV, and the self-consistency convergence criteria for energy tolerance was 10^{-6} eV/atom. Relevant interface models were constructed by

Materials Studio. To ensure adequate space for all atoms and full relaxation of cells, a vacuum layer of 15 Å was reserved for the surface supercell.

3 Results

3.1 Microstructure of Al-Ti-Nb-B alloys

Fig. 3 presents the microstructures of Al-4Ti-1Nb-1B alloys prepared with different Ti and Nb introduction sequences. The alloys primarily contain two secondary phases: MAl_3 (where M = Ti or Nb) and TiB_2 . The composition and morphology of the MAl₃ phase have been analyzed and discussed in our previous study [36]. Therefore, this work focuses on the characterization and analysis of TiB₂ in the different Al-4Ti-1Nb-1B samples. All three preparation methods yield fine, particulate TiB2 phases with particle sizes ranging from approximately 0.5 to 3 µm. There is no significant difference in the size or distribution of TiB₂ particles among the different processing routes. The TiB2 particles exhibit polyhedral morphology, with some degree of agglomeration observed. EDS mappings confirm the overlapping distribution of Ti and B, indicating the formation of TiB₂. Furthermore, both SEM and EDS analyses reveal that TiB₂ particles in all three Al-4Ti-1Nb-1B samples exhibit negligible Nb signals. At this magnification, no evidence of Nb adsorption was observed.

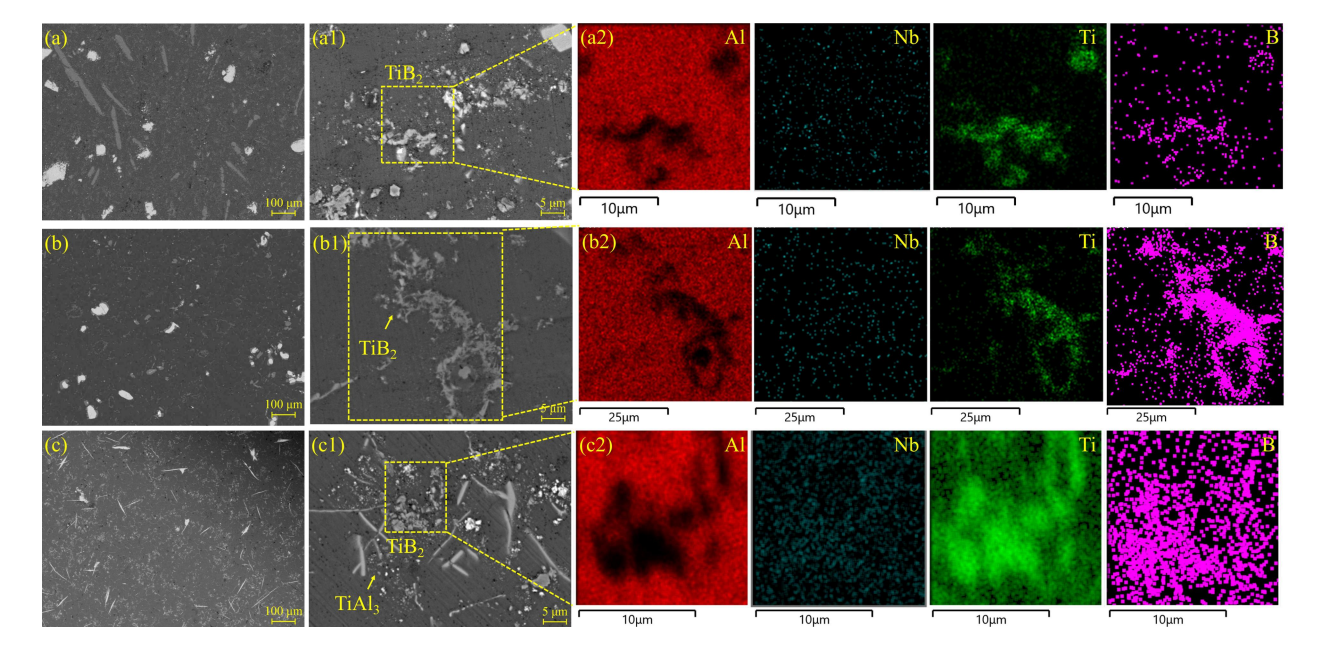


Fig. 3 SEM morphology and EDS mappings of TiB_2 phase in Sample (a-a2) A; (b-b2) B; (c-c2) C.

3.2 Grain refinement effect of Al-Ti-Nb-B alloys

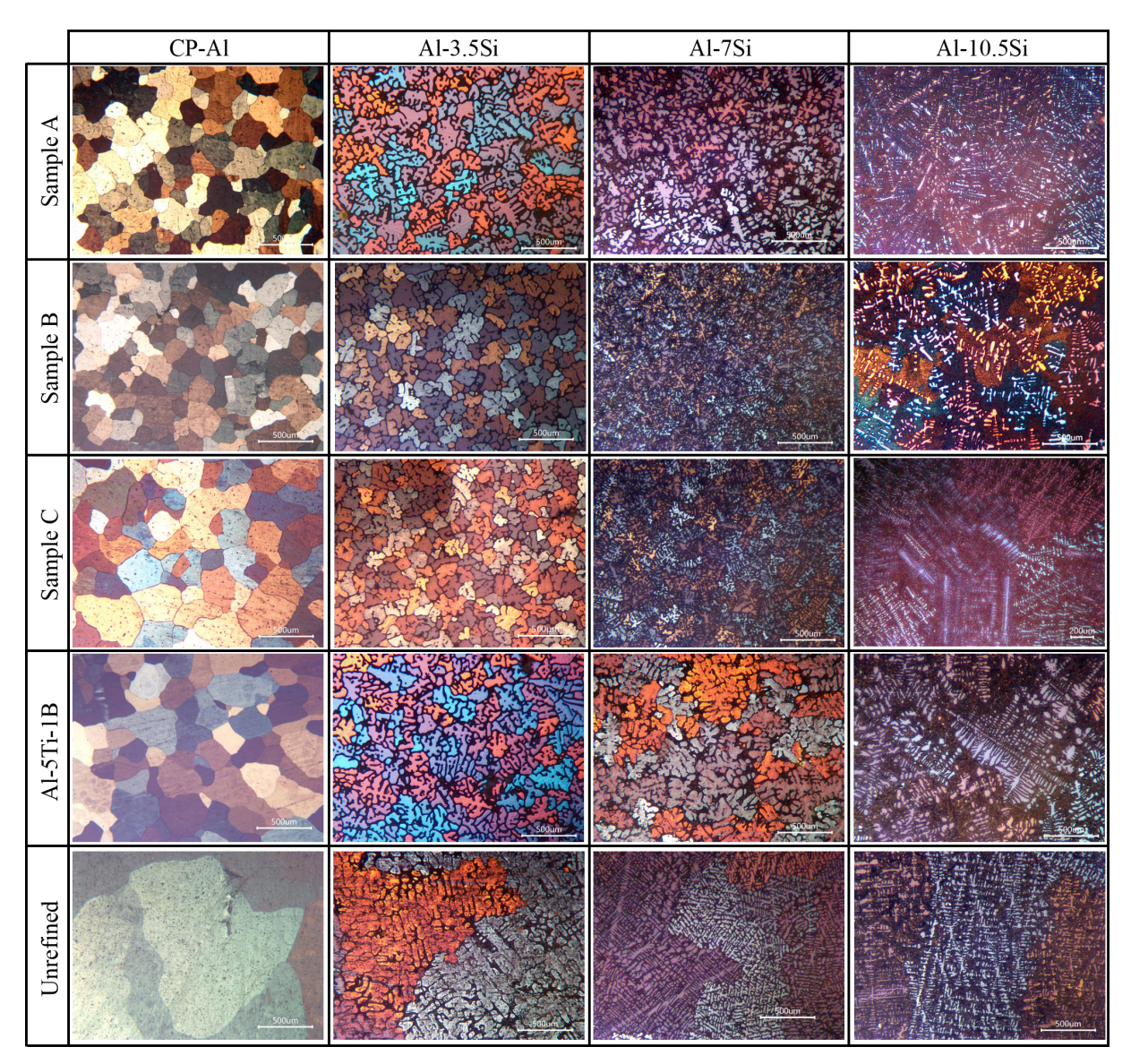


Fig. 4 Polarized morphologies of $\alpha\text{-Al}$ in Al alloys.

Table 2 Average grain sizes (µm) of the Al-7Si alloys with different grain refiners

	CP-Al	Al-3.5Si	Al-7Si	Al-10.5Si
Sample A	176.6±7.1	174.8±6.6	207.8±27.1	472.6±8.2
Sample B	132.3±14.2	148.5±7.7	150.12±27.5	311.1±52.2
Sample C	147.5±20.9	152.7±8.2	180.9±13.6	375.6±65.2
Al-5Ti-1B	175.5±28.1	268.7±45.2	541.1±26.3	559.2±46.6
unrefined	>1500	>1500	>1500	>1500

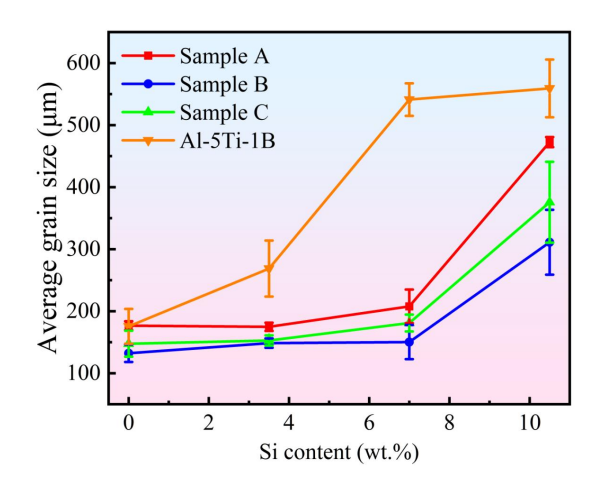


Fig. 5 (a) Grain refinement of Al-Ti-Nb-B with different Nb content.

(b) Grain refinement of Al-4Ti-1Nb-1B with different holding times.

Fig.4 presents the grain refinement results of CP-Al, Al-3.5Si, Al-7Si, and Al-10.5Si alloys inoculated with Sample A, B, C, and commercial Al-5Ti-1B. Table 2 summarizes the α-Al grain size after treatment with various refiners, while Fig. 5 also illustrates the grain refinement size. As shown in Fig. 4, the unrefined alloys (CP-Al, Al-3.5Si, Al-7Si, and Al-10.5Si) exhibit coarse dendritic α-Al grains with average grain size exceeding 1500 µm. Among the refiners tested, Sample B acquires the finest grain sizes: $132.3 \pm 14.2 \,\mu m$ for CP-Al, $148.5 \pm$ 7.7 μm for Al-3.5Si, 150.1 \pm 27.5 μm for Al-7Si, and 311.1 \pm 52.2 μ m for Al-10.5Si. Sample A exhibits slightly inferior refinement compared to Sample B, with grain sizes of 176.6 \pm 7.1 μ m, 174.8 \pm 6.6 μ m, 207.8 \pm 27.1 μ m, and 472.6 \pm 8.2 μ m for CP-Al, Al-3.5Si, Al-7Si, and Al-10.5Si, respectively. Refinement performance of Sample C is intermediate between Samples A and B. Overall, Samples A, B, and C demonstrated superior grain refinement compared to the commercial Al-5Ti-1B refiner.

Notably, for CP-Al and Al-3.5Si alloys, Samples A, B, and C showed comparable and excellent refinement performance. Even commercial Al-5Ti-1B exhibits effective refinement for CP-Al. However, as the Si content increased to 7 wt.%, notable differences in refinement performance among Samples A, B, and C emerges. Sample B significantly outperform Sample C, which in turn was superior to Sample A. At 10.5 wt.% Si, the differences become more pronounced. These results

indicate that at low Si concentrations (0 or 3.5 wt.%), Samples A, B, and C exhibit similarly excellent grain refinement. At higher Si concentrations (7 or 10.5 wt.%), Sample B maintains the strongest resistance to Si poisoning and sustained refinement performance. Sample A shows weaker resistance, and Sample C performs intermediate to A and B.

3.3 Nucleation substrates in the Al-Ti-Nb-B alloys

To further investigate the factors contributing to the grain refinement performance among Samples A, B, and C, TiB₂ particles from each sample were extracted and thinned using focused ion beam (FIB) techniques. Subsequently, STEM combined with EDS was applied to observe the TiB₂ particles in Samples A, B, and C. Fig. 6 summarizes the observations of these particles. Fig. 6(a) shows a block-shaped TiB2 particle from Sample A. The yellow boxed area in Fig. 6(a1) corresponds to the TiB₂/Al interface, where EDS mappings confirm a distinct Nb-enriched layer, indicating Nb adsorption. Analysis of the SAED pattern in Fig. 6(b) and the HRTEM image and EDS line scan in Fig. 6(c) reveal that Nb atoms segregate along the (0110) plane on the TiB₂ surface at the TiB₂/Al interface. Fig. 6(d) presents a stacked, elongated TiB2 particle from Sample B. A pronounced Nb-enriched layer is evident on the TiB2 surface, as shown in Fig. 6(d5). SAED pattern in Fig. 6(e), HRTEM image and EDS line scan in Fig. 6(f) confirm that Nb atoms adsorb along the (0001) plane toward the TiB₂/Al interface. Moreover, Fig. 6(g) depicts a cubic TiB₂ particle from Sample C, with Fig. 6(g1-g5) illustrating Nb adsorption on its surface. The Nb distribution at the TiB₂/Al interface in Sample C is further detailed in Fig. 6(g) and (h).

In summary, all TiB₂ particles from Samples A, B, and C exhibit evident Nb adsorption on the TiB₂/Al interface. Comparative EDS line scans of Nb along the TiB₂/Al interfaces in Fig. 6(c), (f), and (i) indicate that Sample B exhibits the most pronounced Nb adsorption with the highest Nb concentration, followed by Sample C and then Sample A. Correspondingly, Sample B demonstrates superior grain refinement performance across CP-Al, Al-3.5Si, Al-7Si, and Al-10.5Si alloys, especially at higher Si contents (Al-7Si and Al-10.5Si), compared to Samples A and C. Therefore, subsequent analyses focus on the influence of Nb adsorption on the TiB₂ surface on its grain refinement performance.



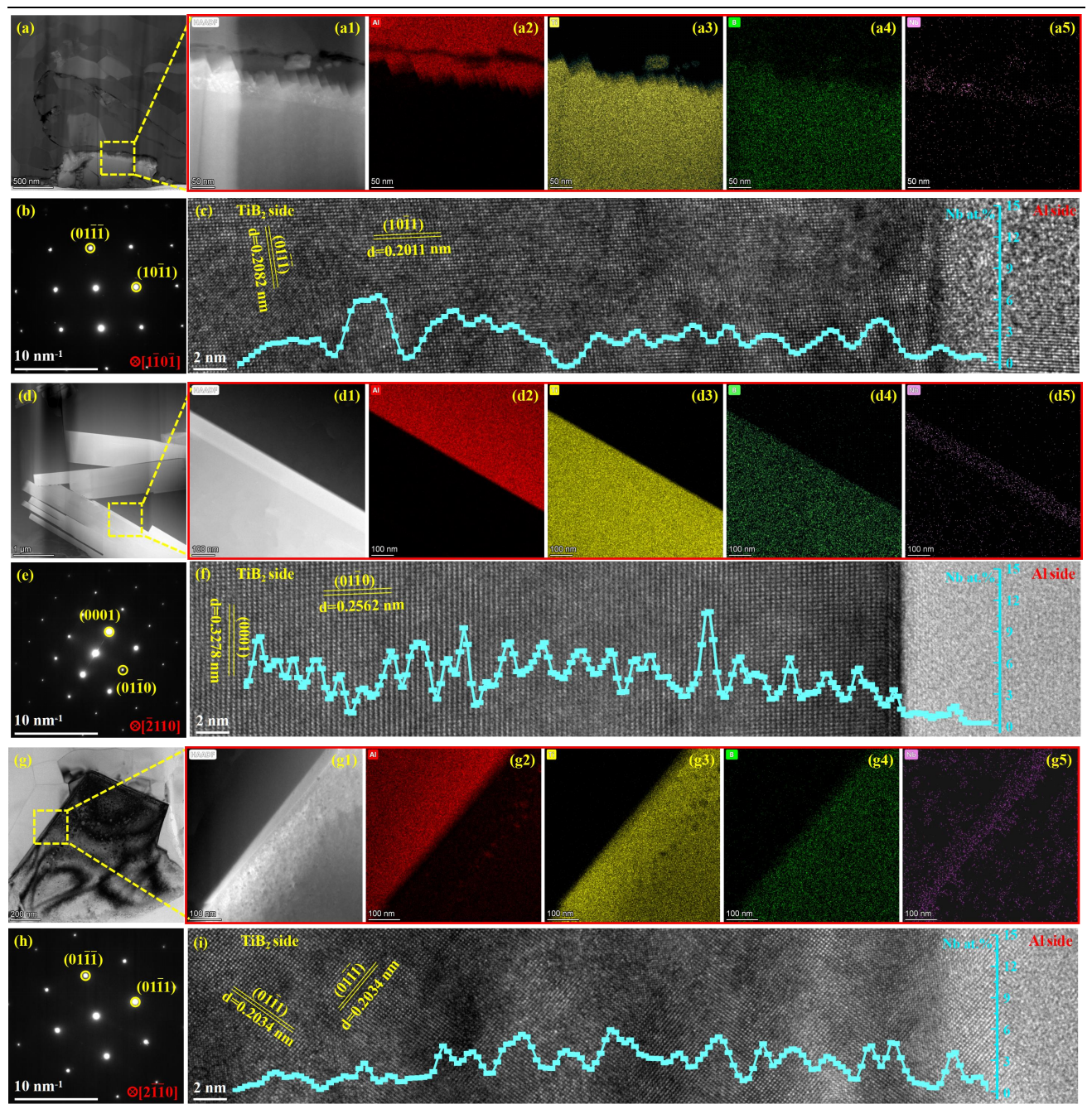


Fig 6 (a-a5) TiB₂ particle in Sample A and corresponding EDS mappings; (b) SAED pattern of the yellow box in (a); (c) HRTEM image of the surface of TiB2 in Sample A and the EDS line-scanning pattern of Nb. (d-d5) TiB2 particle in Sample B and corresponding EDS mappings; (e) SAED pattern of the yellow box in (d); (f) HRTEM image of the surface of TiB2 in Sample B and the EDS line-scanning pattern of Nb. (g-g5) TiB₂ particle in Sample C and corresponding EDS mappings; (h) SAED pattern of the yellow box in (g); (i) HRTEM image of the surface of TiB2 in Sample C and the EDS line-scanning pattern of Nb.

4 Discussion

4.1 Effect of the Ti and Nb introduction sequence on Nb adsorption at the TiB2 surface

In the above experimental investigations, the TiB2 particles in Sample B, prepared by introducing Ti prior to Nb, exhibited the most pronounced Nb surface adsorption. This is considered a major factor contributing to the superior grain refinement performance of Sample B in CP-Al, Al-3.5Si, Al-7Si, and Al-10.5Si alloys. To elucidate the mechanism behind this observation, TiB₂/Al interface models with different Ti and Nb addition sequences are constructed to investigate their influence on Nb adsorption behavior at the TiB2 surface.

According to the process shown in Fig. 1(b), during the 60 min holding period at 900 °C after the addition of the Al-Ti alloy, the melt environment contains insoluble TiB₂ particles and excess Ti and Al. This condition resembles that used in the preparation of Al-Ti-B grain refiners. Based on the work by Fan et al. [37, 38], such an environment facilitates the formation of a two-dimensional TiAl₃ compound (TiAl₃ 2DC) on the (0001) surface of TiB₂. Following this, Nb is introduced. Driven by the tendency of the TiB2/Al interface to evolve toward a thermodynamically stable state, Nb atoms may diffuse through the TiAl₃ 2DC layer and subsequently enter the TiB₂ particles, resulting in interface reconstruction. Our previous study confirmed that in the presence of excess Nb in the melt, a NbAl₃ 2DC layer can form at the TiB₂ surface [29]. Fig. 7(a1-a3) illustrates this evolution process. TiB₂ initially coated with a TiAl₃ 2DC layer undergoes Nb diffusion into the 2DC, forming NbAl₃ 2DC, followed by further Nb diffusion into the TiB₂ particles, ultimately producing Nb surface adsorption.

In contrast, when TiB₂ is synthesized in situ prior to Ti and Nb addition, as shown in Fig. 1(a), the Ti:B ratio is controlled at 2.2, and the reaction is maintained for 30

min. No excess Ti remains in the melt to form a TiAl₃ 2DC layer. When Nb is introduced first under these conditions, Nb atoms gradually diffuse directly to the TiB₂ surface and progressively incorporate into it, resulting in Nb adsorption.. Therefore, Fig. 7(b1-b3) illustrates the interface evolution under the Nb-first route. The ground-state energies for both addition sequences are calculated using the ab initio method and are summarized in Fig. 7(c). It is evident that the Ti-first followed by Nb introduction sequence results in a smaller ground-state energy change (ΔE), along with lower intermediate energy levels and a stronger driving force. This indicates that Nb adsorption on the TiB₂ surface under this sequence is more thermodynamically favorable. Consequently, Sample B exhibits the most pronounced Nb adsorption on the TiB2 surface, followed by Sample C, while Sample A shows the weakest adsorption.

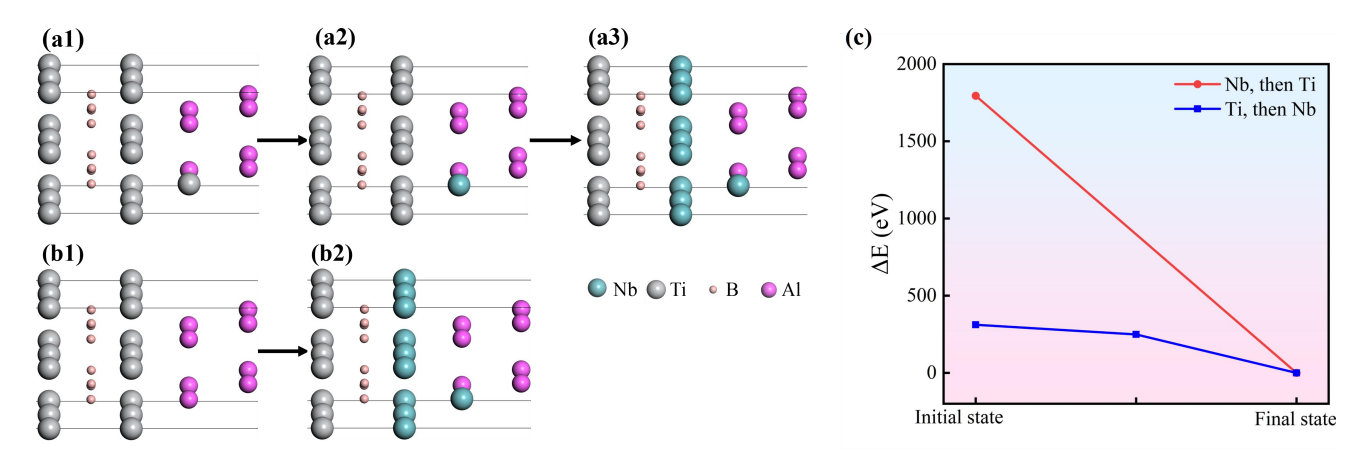


Fig. 7 (a1-a3) Reconstruction of the TiB₂/Al interface under the introduction sequence of Ti followed by Nb. (b1-b2) Reconstruction of the TiB₂/Al interface under the introduction sequence of Nb followed by Ti. (c) Energy variation, ΔE, induced by the introduction sequence of Ti and Nb.

4.2 Effect of Nb adsorption amount on grain refinement performance and Si-poisoning resistance

The grain refinement results shown in Fig. 4 demonstrate that Sample B exhibits superior refinement efficiency for CP-Al, Al-3.5Si, Al-7Si, and Al-10.5Si compared to Samples A and C. The Nb elemental line scans presented in Fig. 6(c), (f), and (i) reveal significant differences in Nb adsorption at the TiB₂ surfaces among the three samples. The corresponding Nb line scan profiles for Samples A, B, and C are compared in Fig. 8, with their average and maximum Nb concentrations summarized in Table 3. Sample B shows the highest Nb surface adsorption on TiB₂, with an average Nb content of 3.80

at.%, which significantly exceeds the critical threshold of 1.92 at.% previously reported to activate TiB₂ as an effective nucleation site [36]. Sample C exhibits a moderate Nb adsorption level of 2.38 at.%, while Sample A presents the lowest, at only 2.03 at.%. Although all three samples outperform the commercial Al-5Ti-1B refiner in refining CP-Al and various Al-Si alloys, the grain refinement performance of Sample B is clearly superior to that of Sample C, and markedly better than that of Sample A. Therefore, the influence of Nb adsorption content at the TiB₂ surface on grain refinement and Si-poisoning resistance is investigated in detail.

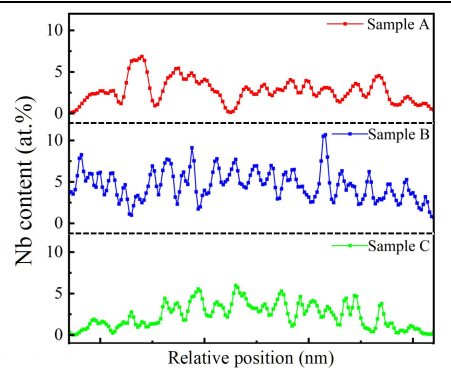


Fig. 8 The EDS line-scanning patterns showing the composition profiles of Nb on the surface of TiB₂

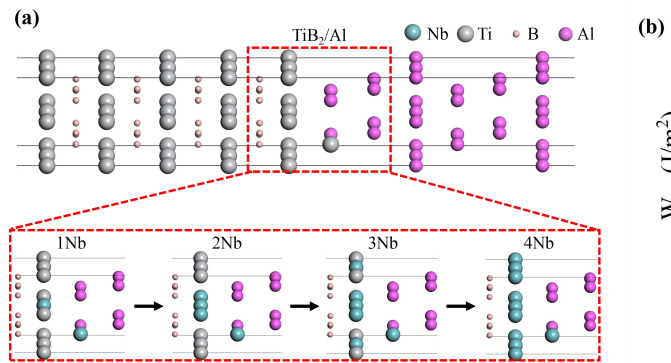
Table 3 Nb content on the surface of TiB2 in Al-Ti-Nb-B

Grain	Average Nb content	Maximum Nb content	
refiner	(at.%)	(at.%)	
Sample A	2.03	6.85	
Sample B	3.80	10.68	
Sample C	2.38	5.98	

To quantify the nucleation tendency of α -Al on the TiB₂ surface, the adhesion energy $W_{\rm ad}$, which represents the work required to separate one interface into two free surfaces, is calculated using the following equations^[39,40]:

$$W_{ad} = \frac{1}{A} \left(E_{slab}^{Al} + E_{slab}^{TiB_2} - E_{interface} \right) \tag{9}$$

where $E_{interface}$, E_{slab}^{Al} and $E_{slab}^{TiB_2}$ are calculated by the ab initio method, denoting the ground state energies of the interface model, the Al, and the substrate slab, respectively. Wad denotes the adhesion energy of the TiB₂/Al and interface. A denotes the interfacial area of the TiB₂/Al interface. Various TiB₂/Al interfaces incorporating different numbers of Nb atoms are constructed, as shown in Fig. 9. For comparison, the TiB₂/Al interface from commercial Al-5Ti-1B was also modeled, based on previous studies [37, 41, 42]. The adhesion energies, W_{ad} , of the corresponding interface models are calculated and presented in Fig. 9(b). The adhesion energy of the TiB₂/Al interface without Nb atoms is 3.72 J/m², which is in good agreement with the result reported by Li et al. (3.77 J/m²) [25]. For comparison, the W_{ad} of the TiB₂/Al interface with one Nb atom increases to 3.93 J/m². With the adsorption of two Nb atoms, $W_{\rm ad}$ increases to 3.96 J/m². The adhesion energies of TiB₂/Al interfaces with three and four Nb atoms are 3.97 and 3.95 J/m², respectively. These results clearly demonstrate that the presence of Nb atoms at the TiB₂/Al interface significantly enhances the adhesion energy, indicating a strong tendency to form a more stable interface. Thus, the Nb adsorption at the TiB2 surface is the key factor contributing to the superior grain refinement performance of Samples A, B, and C.



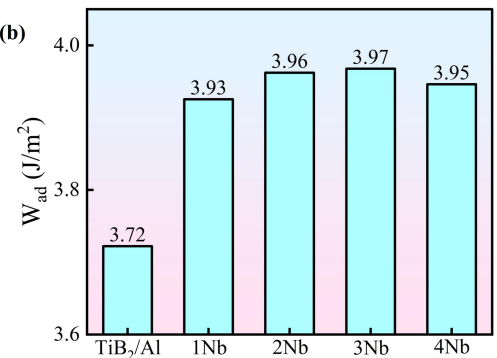


Fig. 9 Effect of Nb adsorption at TiB₂/Al interface on the adhesion energy Wad. (a) TiB₂/Al interface models with various Nb atoms. (b) Variation of the adhesion energy Wad of corresponding structures.

In addition, the superior resistance to Si poisoning of Sample B is a critical distinguishing feature, compared to Samples A and C. It is important to investigate the influence of Nb adsorption on Si atoms at the TiB2 surface. To quantitatively compare the Si adsorption propensity at TiB2/Al and TiB2(Nb)/Al interfaces , the Si adsorption factor $\kappa_{Si}(c_{Si})$ is defined [25]

$$\kappa_{Si}(c_{si}) = \frac{W_{ad(c_{si})}}{W_{ad(0)}} \tag{10}$$

where $W_{\rm ad(CSi)}$ and $W_{\rm ad(0)}$ denote the adhesion energies when the Si concentration at the interface is $c_{\rm Si}$ and 0, respectively. The TiB₂/Al interfaces with adsorbed Si atoms and their corresponding segregation tendency, denoted as $\kappa_{\rm Si}(c_{\rm si})$, are presented in Fig. 10. As the interfacial Si concentration, $c_{\rm Si}$, increases, $\kappa_{\rm Si}(c_{\rm si})$ of TiB₂/Al, TiB₂/Al with 1 Nb atom, and TiB₂/Al with 2 Nb atoms rises, indicating a higher tendency for Si segregation at higher concentrations. However, $\kappa_{\rm Si}(c_{\rm si})$ is lower for TiB₂/Al interfaces with 2 Nb atoms than with 1

Nb, and both are lower than the Nb-free interface, suggesting that greater Nb segregation reduces Si accumulation. For TiB₂/Al interfaces with 3 or 4 Nb atoms, $\kappa_{Si}(c_{si})$ reaches a maximum at $c_{Si} = 0.75$ and then decreases as c_{Si} increases to 1, indicating that further Si enrichment becomes increasingly difficult at higher Nb concentrations. Furthermore, $\kappa_{Si}(c_{si})$ consistently decreases with increasing

Nb content from 1 to 4 Nb atoms under the same $c_{\rm Si}$, reinforcing the conclusion that higher Nb adsorption at the TiB₂/Al interface suppresses Si segregation. These findings explain why Sample B, which exhibits the highest Nb adsorption content at the TiB₂ surface, achieves superior refinement performance in Al-7Si and Al-10.5Si alloys compared to Samples A and C.

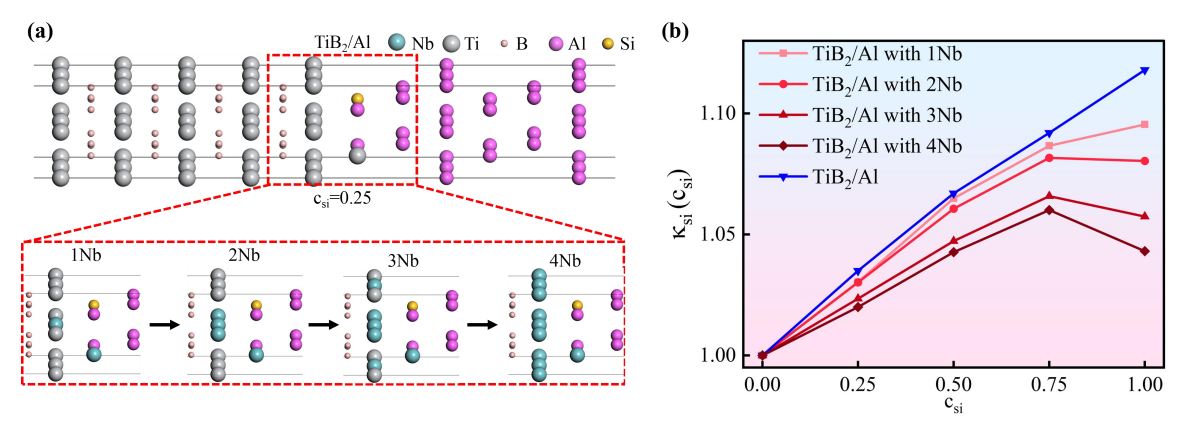


Fig. 10 Effect of Nb adsorption at TiB₂/Al interface on Si segregation propensity, $\kappa_{Si}(c_{si})$. (a) TiB₂/Al interfaces with various Nb atoms and Si segregation. (b) Variation of $\kappa_{Si}(c_{si})$ for corresponding interfaces.

In summary, the enhanced grain refinement and Si-poisoning resistance in Sample B can be attributed to the higher Nb adsorption at the TiB₂ surface. As shown in Fig. 11, Ti is first introduced to form a Ti-rich Al-Ti-B melt. Nb is then added, and through substitution of Ti in the TiAl₃ 2DC layer and subsequent diffusion, Nb atoms are incorporated into the TiB₂ surface, leading to a significant content of Nb adsorption. This unique Nb

adsorption increases the interfacial adhesion energy W_{ad} and reduces the Si segregation tendency $\kappa_{Si}(c_{si})$ at the TiB₂/Al interface. The higher the Nb content at the interface, the stronger the resistance to Si poisoning. The superior performance of Sample B is thus attributed to an average Nb content of 3.80 at.%, which optimizes both grain refinement and resistance to Si poisoning.

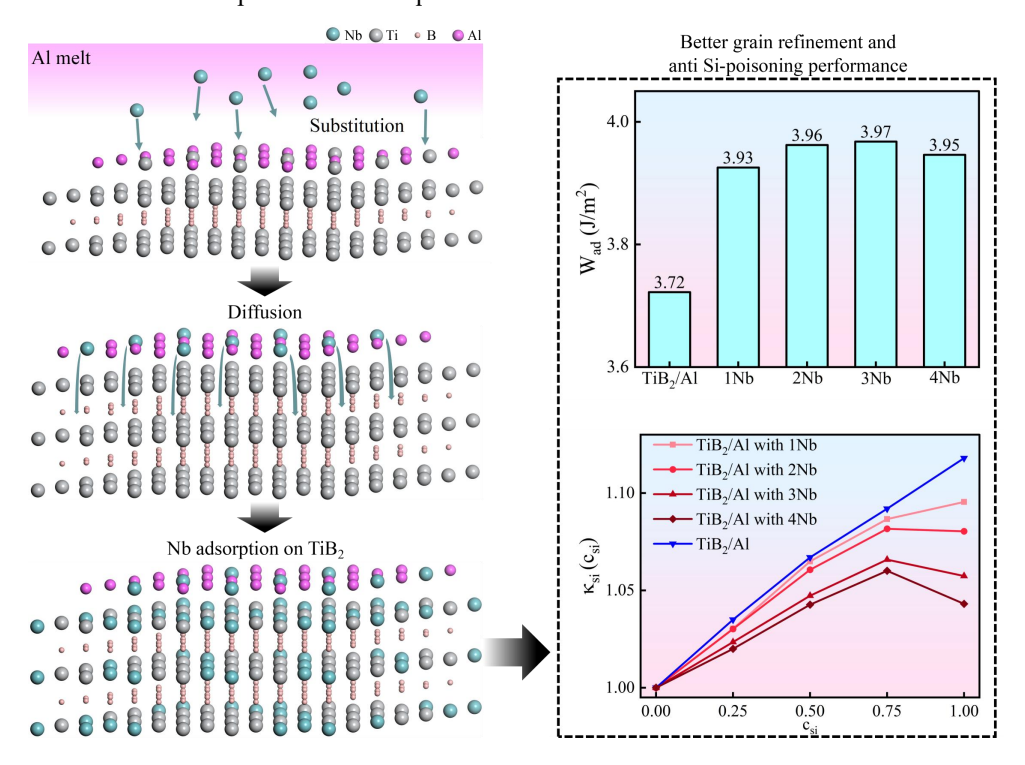


Fig. 11 A schematic illustration of the Nb adsorption mechanisms on TiB₂

5 Conclusions

In this study, a series of Al-4Ti-1Nb-1B grain refiners were prepared via different sequences for introducing Ti and Nb. It was found that the sequence of Ti and Nb addition significantly influences the adsorption behavior of Nb at the TiB₂ surface, thereby affecting both the grain refinement efficiency and resistance to Si poisoning. The following conclusions can be drawn:

(1)All Al-4Ti-1Nb-1B refiners, regardless of the Ti and Nb addition sequence, exhibited excellent grain refinement performance in low-Si aluminum alloys such as CP-Al and Al-3.5Si. For high-Si alloys such as Al-7Si and Al-10.5Si, the refiner synthesized by first adding Ti followed by Nb demonstrates the best refinement performance, refining the α -Al grain size of Al-7Si to $150.12 \pm 27.5 \ \mu m$.

(2)Introducing Ti prior to Nb lead to the most pronounced Nb adsorption at the TiB_2 surface. Initially, Ti promotes the formation of a $TiAl_3$ 2DC on the in-situ formed TiB_2 . Subsequently, due to thermodynamic driving forces favoring lower ground-state energy, Nb atoms replace Ti in the surface $TiAl_3$ 2DC and gradually diffuse into the TiB_2 , forming a stable Nb-enriched layer. The ground-state energy change ΔE for the Ti prior to Nb process is lower than that of the reverse sequence, making Nb adsorption more favorable in this route.

(3) Varying degrees of Nb adsorption are observed at the TiB₂ surface. The highest concentration, 3.80 at.%, is obtained in the sample introducing Ti prior to Nb. First-principles calculations revealed that higher Nb content enhance the TiB₂/Al interfacial adhesion energy $W_{\rm ad}$ and suppress the segregation tendency of Si atoms, represented by $\kappa_{\rm Si}(c_{\rm si})$. The Nb adsorption at the TiB₂ surface is thus the key factor contributing to the superior performance of the Al-4Ti-1Nb-1B refiners. A higher level of Nb adsorption at the TiB₂ surface leads to improved refinement performance and stronger Si-poisoning resistance, particularly in high-Si alloys such as Al-7Si and Al-10.5Si.

Acknowledgements

The authors gratefully acknowledge financial support by "the Fundamental Research Funds for the Central Universities" (YWF-22-L-1284, YWF-23-Q-1097).

Author information

First author: Yi Hao, male, born in 1997, Ph.D. candidate, e-mail: yihao@buaa.edu.cn

Corresponding author 1: Zhang Huarui, female, born in 1984, associate professor, e-mail: huarui@buaa.edu.cn

Corresponding author 2: Cheng Ying, male, born in 1991, Ph.D., e-mail: cying@buaa.edu.cn

Address: Shahe Campus, Beihang University, Changping District, Beijing

Reference

- [1] Easton M A, Qian M, Prasad A, et al. Recent advances in grain refinement of light metals and alloys[J] .Current Opinion in Solid State & Materials Science, 2016, 20(1):13-24.
- [2] Feng Wang, Yulung Chiu, Dmitry Eskin, et al. A grain refinement mechanism of cast commercial purity aluminium by vanadium[J]. Materials Characterization, 2021, 181:111468.
- [3] ASM Handbook Volume 15: Casting, ASM International 2008.
- [4] D. Stjohn, M. Easton, M. Qian, J. Taylor. Grain refinement of magnesium alloys: a review of recent research, theoretical developments and their application[J]. Metallurgical and Materials Transactions A, 2013, 44(7):2935-2949.
- [5] F. Robles, J. Hernandez, R. M. Ramirez. Al-Si Alloys: Automotive, Aeronautical, and Aerospace Applications[J]. Springer International Publishing AG, 2017.
- [6] B. Murty, S. Kori, M. Chakraborty. Grain refinement of aluminium and its alloys by heterogeneous nucleation and alloying [J]. Metallurgical Reviews, 2002, 47(1):3-29.
- [7] G.P. Jones, New ideas on the mechanism of heterogeneous nucleation in liquid aluminium, National Physical Laboratory Division of Chemical Standards 1980.
- [8] A. Greer, A. Bunn, A. Tronche, et al. Modelling of inoculation of metallic melts: application to grain refinement of aluminium by Al-Ti-B[J]. Acta Materialia, 2000, 48(11):2823-2835.
- [9] Y. Li, B. Hu, B. Liu, et al. Insight into Si poisoning on grain refinement of Al-Si/Al-5Ti-B system[J]. Acta Materialia, 2020, 187: 51-65.
- [10] Birol Y. Effect of silicon content in grain refining hypoeutectic Al-Si foundry alloys with boron and titanium additions[J]. Materials Science & Technology, 2014, 28(4):385-389.
- [11] T. Quested, A. Dinsdale, A. Greer. Thermodynamic evidence for a poisoning mechanism in the Al-Si-Ti system[J]. Metal Science Journal, 2013, 22(9): 1126-1134.
- [12] Y. Wang, Z. Que, T. Hashimoto, et al. Mechanism for Si Poisoning of Al-Ti-B Grain Refiners in Al Alloys[J]. Metallurgical and Materials Transactions A, 2020, 51(11):1-15.
- [13] L. Bolzoni, N. Babu. Refinement of the grain size of the LM25 Alloy (A356) by 96Al-2Nb-2B Master Alloy[J]. Journal of Materials Processing Tech, 2015, 222:219-223.
- [14] L. Bolzoni, M. Nowak, N. Babu. Grain refinement of Al-Si alloys by Nb-B inoculation. Part II: Application to commercial alloys[J]. Materials & Design, 2015,

66:376-383.

- [15] L. Bolzoni, M. Nowak, N. Babu. Assessment of the influence of Al-2Nb-2B master alloy on the grain refinement and properties of LM6 (A413) alloy[J]. Materials Science & Engineering A, 2015, 628(mar.25): 230-237
- [16] Y. Li, Y. Jiang, B. Liu, et al. Understanding grain refining and anti Si-poisoning effect in Al-10Si/Al-5Nb-B system[J]. Journal of Materials Science & Technology, 2021, 65: 190-201.
- [17] J. Zhao, M. Jackeson, L. Peluso. Mapping of the Nb-Ti-Si phase diagram using diffusion multiples[J]. Materials Science and Engineering: A, 2004.
- [18] Y. Li, B. Hu, Q. Gu. Achievement in grain-refining hypoeutectic Al-Si alloys with Nb[J]. Scripta Materialia, 2019, 160: 75-80.
- [19] J. Xu, R. Li, Q. Li. Effect of Agglomeration on Nucleation Potency of Inoculant Particles in the Al-Nb-B Master Alloy: Modeling and Experiments[J]. Metallurgical and Materials Transactions A, 2021, 52(3).
- [20] J. Xu, Y. Li, B. Hu. Development of Al-Nb-B master alloy with high Nb/B ratio for grain refinement of hypoeutectic Al-Si cast alloys[J]. Journal of Materials Science, 2019, 54(23):14561-14576.
- [21] J. Xu, Y. Li, K. Ma. In-situ observation of grain refinement dynamics of hypoeutectic Al-Si alloy inoculated by Al-Ti-Nb-B alloy[J]. Scripta Materialia, 2020, 187: 142-147.
- [22] Y. Li, Y. Jiang, B. Hu. Novel Al-Ti-Nb-B grain refiners with superior efficiency for Al-Si alloys[J]. Scripta Materialia, 2020, 187(1): 262-267.
- [23] L. Zhu, Y. Zhang, Q. Li. Effectively refining Al-10Si alloy via Al-Ti-Nb-B refiner with Nb₂O₅[J]. Journal of Materials Science & Technology, 2024, 176(9):204-210.
- [24] D. Wu, S. Ma, T. Jing. Revealing the mechanism of grain refinement and anti Si-poisoning induced by (Nb, Ti)B₂ with a sandwich-like structure[J]. Acta Materialia, 2021, 219: 117265
- [25] D. Li, X. Yan, Y. Fan. An anti Si/Zr-poisoning strategy of Al grain refinement by the evolving effect of doped complex[J]. Acta materialia, 2023, 249: 118812.
- [26] D. Li, K. Zhao, X. Liu. Revealing the correlation of microstructure configuration and mechanical properties of Al-Si-Mg alloy reinforced by C-doped TiB₂ and SiC[J]. Materials Design, 2023, 226: 111694.
- [27] D. Li, K. Zhao, M. Han. Optimizing microstructure and enhancing mechanical properties of Al-Si-Mg-Mn-based alloy by novel C-doped TiB₂ particles[J]. Journal of Materials Research and Technology, 2023, 26(000):17.
- [28] L. Xue, h. Jia, P. Ma. Influence of V/B ratio and rolling treatment on the grain refinement efficacy and anti-fading ability of Al-V-B master alloys[J]. Materials Characterization, 2025, 219: 114596.

- [29] H. Yi, Y. Cheng, H. Zhang. Simultaneous integration of anti Si-poisoning and anti-fading properties on an innovative Al grain refiner via Nb-modified TiB₂[J]. Journal of Alloys and Compounds, 2024, 995, 174707.
- [30] Trujillo, Javier F. A strict formulation of a nonlinear Helmholtz equation for the propagation of sound in bubbly liquids. Part I: Theory and validation at low acoustic pressure amplitudes[J]. Ultrasonics Sonochemistry, 2018, 47:75-98.
- [31] PE. Blochl, Projector augmented-wave method[J]. Physical Review B, 1994, 50: 17953-17979.
- [32] G. Kresse, J. Hafner, Ab initio molecular-dynamics simulation of the liquid-metal-amorphous-semiconductor transition in germanium[J], Physical Review B, 1994, 49:14251.
- [33] G. Kresse, J. Furthmuller, Efficient iterative schemes for ab initio total-energy calculations using a plane-wave basis set[J], Physical Review B, 1996, 54: 11169-11186.
- [34] J. Perdew, K. Burke, M. Ernzerhof. Generalized Gradient Approximation Made Simple[J]. Physical Review Letters, 1998, 77(18): 3865-3868.
- [35] G. Kresse, D. Joubert. From ultrasoft pseudopotentials to the Projector Augmented-Wave Method[J], Physical Review B, 1999, 59: 1758-1775.
- [36] H. Yi, Y. Cheng, H. Zhang. Nb adsorption effect and mechanism on Al/TiB₂ interface in novel low-Nb Al-Ti-Nb-B grain refiner[J]. Applied Surface Science, 2025, 710. 164005.
- [37] Z. Fan, Y. Wang, Y. Zhang.Grain refining mechanism in the Al/Al-Ti-B system[J]. Acta Materialia, 2015, 84, 292-304.
- [38] H. Men, Z. Fan. Effects of solute content on grain refinement in an isothermal melt[J]. Acta Materialia, 2011, 59, 2704-2712.
- [39] L. Liu. First-principles study of polar Al/TiN(111) interfaces[J]. Acta Materialia, 2004, 52(12):3681-3688.
- [40] D. Siegel, L. Hector, J. Adams. First-principles study of metal-carbide/nitride adhesion: Al/VC vs. Al/VN[J]. Acta Materialia, 2002, 50(3):619-631.
- [41] H. Men H, Z. Fan. Atomic ordering in liquid aluminium induced by substrates with misfits[J]. Computational Materials Science, 2014, 85:1-7.
- [42] Z. Fan, Y. Wang, M. Xia. Enhanced heterogeneous nucleation in AZ91D alloy by intensive melt shearing[J]. Acta Materialia, 2009, 57(16): 4891-4901.